Transcranial Direct Current Stimulation (tDCS): Predicted Current Densities in a Realistic Head Model

Rosalind J Sadleir[1], PhD, Tracy D Vannorsdall[2], PhD, David J Schretlen[2,3], PhD, Barry Gordon[4,5], MD, PhD

[1]Pruitt Family Department of Biomedical Engineering, University of Florida, [2]Psychiatry & Behavioral Sciences, [3]Russell H. Morgan Department of Radiology & Radiological Science, [4]Neurology, The Johns Hopkins University School of Medicine, [5]Cognitive Science, The Johns Hopkins University

Abstract

tDCS has been used increasingly for clinical and research purposes. It has been assumed that the most significant current densities occur in brain regions underneath the stimulating electrodes and that these regions are physiologically most relevant. We simulated current densities achieved in the entire cerebrum with a commonly used electrode pattern ("stimulation" electrode at F3, "reference" electrode in the right supraorbital region), using a finite-element model based on a realistic human head phantom, 10 different tissue types, and a range of white matter conductivities. The F3-RS arrangement produced relatively large current densities under electrodes; cerebral current densities were higher in the right than left prefrontal areas near the "active" electrode. Other cerebral structures experienced potentially significant current flows. This dependence was confirmed in a second simulation using F4 and left supraorbital positions, where large currents were observed in left prefrontal regions. Because the mechanism(s) of tDCS are not completely known, these simulations suggest we should consider that behavioral effects may originate in regions other than those putatively targeted. They also offer the possibility that other, possibly non-intuitive electrode placements may allow more specific targeting of current flow.

Introduction

Transcranial Direct Current Stimulation (tDCS) involves the application of relatively weak direct current to the brain through the scalp with the aim of modulating underlying cerebral function. Typically, current is introduced through a relatively large (ca. 35 cm^2) sponge electrode over the region to be stimulated, using a constant current stimulator (e.g. Wagner et al. 2007). A reference sponge electrode of similar size is placed elsewhere to complete the circuit. Over the last several years, tDCS has become increasingly popular as a research tool and as a potential therapeutic method for a variety of functions, ranging from basic motor activities (Nitsche and Paulus 2000) through semantic processing and executive function (Fregni et al. 2005, Wasserman and Grafman 2005, Sparing and Mottaghy 2008).

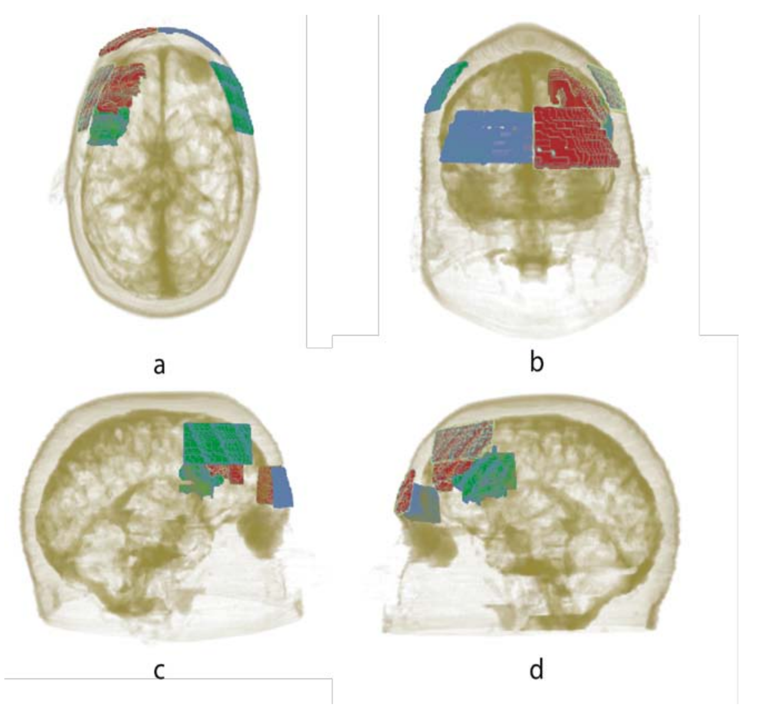

Figure 1. 3D images of (A) transverse, (B) coronal, (C) right saggital and (D) left saggital views of electrodes (22 cm^2 area) placed at F3, F4 and left and right supraorbital regions, superimposed on a shadowed head model. The left inferior frontal gyri and left DLPFC are highlighted in the interior.

In this study, we present a more refined model of current flow in the human brain, by (a) simulating current flow in the entire human head and brain, (b) using a finite element model derived from a segmented whole-head MRI data set, (c) using resistivities from empirical measures of a larger number of conductivity elements than have been used previously, (d) examining current density distributions in structures that, although experiencing lower current densities than "target" regions, may contribute to observed effects and (e) determining the sensitivity of the results to changes in conductivity value by varying white matter conductivity by a factor of 10. The tDCS conditions we modeled were with the "stimulating" electrode placed over F3, and the "reference" electrode over a right supraorbital (RS) location, as well as the complements of these locations (stimulating electrode over F4, reference over the left supraorbital region).

We chose these locations to simulate based upon a number of factors. One was the clear anatomical and presumed functional distinction between the structures that might be activated by these electrode locations. The other major factor was the existence of an empirical literature examining aspects of working memory and language that have used precisely these locations (Fregni et al. 2005, Iyer et al. 2005).

Methods

Our model was based on the Zubal phantom (Zubal et al. 1994). This three-dimensional representation of an adult human head comprises 62 manually segmented compartments. Data for the Zubal phantom were obtained from a 1.5-T MRI scan of a normal man. Slices spanned the head from its apex to the roof of the mouth. The overall model had 120 axial slices containing tissue, each slice having 256 x 256 voxels. The overall dimensions of the model were 28.2 cm x 28.2 cm in each transverse plane and 16.8 cm axially. The total volume of tissue in the model was 3682 ml. Each voxel had dimensions of 1.1 mm x 1.1 mm in the transverse plane and a thickness of 1.4 mm. We defined ten electrically significant tissues within the model: bone, scalp, blood, CSF, muscle, white matter, gray matter, sclera, fat and cartilage, with conductivity values chosen, where possible, from reliable reported low frequency values at less than 1 kHz. No anisotropy was assigned to the brain compartments, skull, or muscle. Instead, a composite value derived from longitudinal and transverse conductivities was applied to white matter and muscle tissue. We also compared the results from this composite value with this intermediate white matter value replaced with literature values measured transverse or longitudinal to white matter fibers to determine the sensitivity of results to the conductivities chosen.

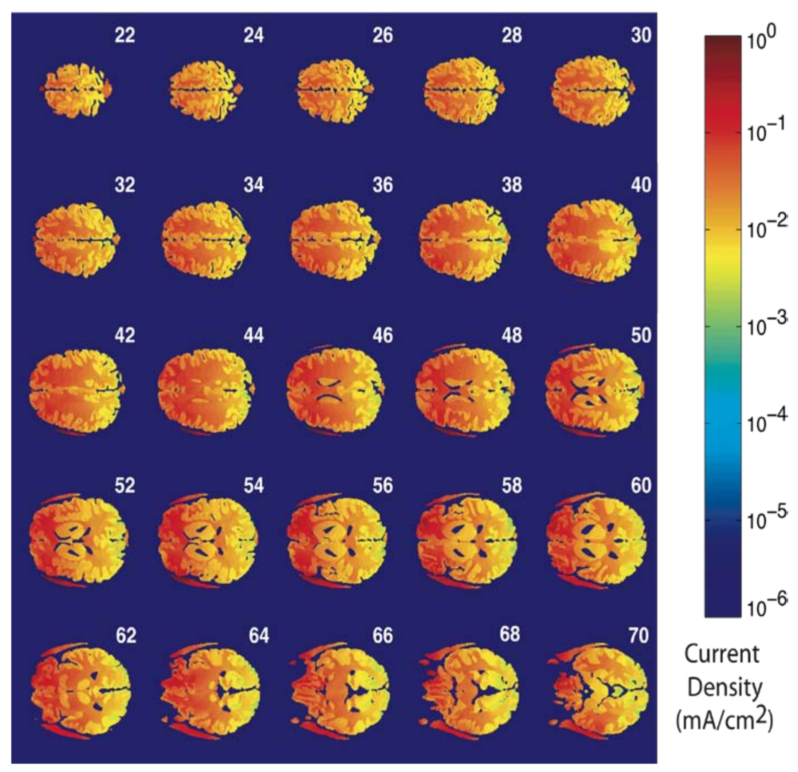

Figure 2. Transverse slices of current density formed between 22 cm^2 electrodes placed at F3 and RS at 1 mA current. Fat, CSF, skull, and skin tissues have been masked out of the images to allow comparison of current densities in interior tissue only. Slice numbers are marked in the upper right-hand corner of each image, with slice number increasing axially from the head apex. Higher current densities are visible in right frontal areas in slices 56, 58, 60 and 62.

Finite Element Model and Electrode Assignment

The Zubal phantom was directly translated to a 3D conductivity volume and converted into a linear rectangular prismatic finite element model. The model contained approximately 2.2 million elements. The model solved the equation

$$\nabla \cdot \left(\sigma(x,y,z)\,\nabla\phi\right) = 0 \qquad (1)$$

on the domain Ω (the head), subject to

$$\sigma\frac{\partial\phi}{d\mathbf{n}} = j \ \text{ and } \sum_{d\Omega} j = 0 \qquad (2)$$

where $d\Omega$ is the head surface, ϕ is the voltage distribution, j is the surface current density and **n** is a vector normal to the surface. The quantity σ is the conductivity distribution within the head. The total current injected into the head was 1 mA in both electrode configurations, with the injected current density used being approximately 45 mA/cm^2 for each configuration. We adopted the protocol used in several published studies (Iyer et al. 2005, Fregni et al. 2005) and located simulated electrodes of approximately one voxel (1.1 mm) thickness and 1 S/m conductivity centered over F3 in the 10-20 electrode system (over the left posterior inferior frontal region) and at a right supraorbital location on the phantom.

We also examined results of using a second pair of simulated electrodes with the same surface area, with locations mirroring the first and accordingly placed at approximately F4 and a left supraorbital (LS) location. Each electrode had an area of 22 cm^2 (although their shapes were slightly different). Placement of the F3-RS montage is shown in Figure 1 compared to locations of the left IFG and DLPFC.

Analysis of regions of interest

Regions of particular interest were identified: 5 anatomically-defined brain regions (prefrontal, frontal, parietal, temporal and occipital); 8 areas generally thought to be of special importance for learning memory and language (IFG, DLPFC, hippocampus, globus pallidus, septum pellucidum, caudate nucleus, putamen and amygdala); and 9 of the ten electrically distinct tissue types (fat, bone, cerebrospinal fluid (CSF), cartilage, scalp, white matter, gray matter, sclera and muscle). The tenth tissue, blood, only constituted 24 ml of the model volume and was omitted from the analysis. We investigated and analyzed current density distributions within each of these regions and tissue types. In order to compare our modeling results with experimental observations, we also examined current density distributions near the retina and optic nerve in order to try to relate these to the likelihood of phosphene production. We found that current density distributions were approximately log-normal. We constructed histograms of logged current density distributions within regions and compared median current density differences between different stimulation paradigms using Mann-Whitney U-tests, adopting α = .05 in all cases.

Results

Maximal current densities observed within the head were of the order of 0.8 mA/cm^2. Figure 2 shows log-scaled current densities in cerebral tissue resulting from the F3-RS electrode placement, and with skin, skull, fat and CSF current densities masked out. Large current densities were evident in both left and right areas adjacent to the anode and cathode. Larger current densities are apparent in the right frontal area than in either left frontal or prefrontal areas. This can be clearly discerned in images of slices 56, 58 60 and 62.

As expected, current densities in those tissues such as skin, muscle and CSF directly subjacent to electrodes were large. The current density in right eye scleral tissue was particularly high. Current densities in other tissues near electrodes such as fat and bone were comparatively low because of their lower conductivities. Regions generally considered more relevant to language, learning and memory (Figure 3) experienced moderate current densities, with those in IFG and DLPFC having the largest densities of these regions. Less current was present in the occipital lobes than in more frontal areas (Figure 4).

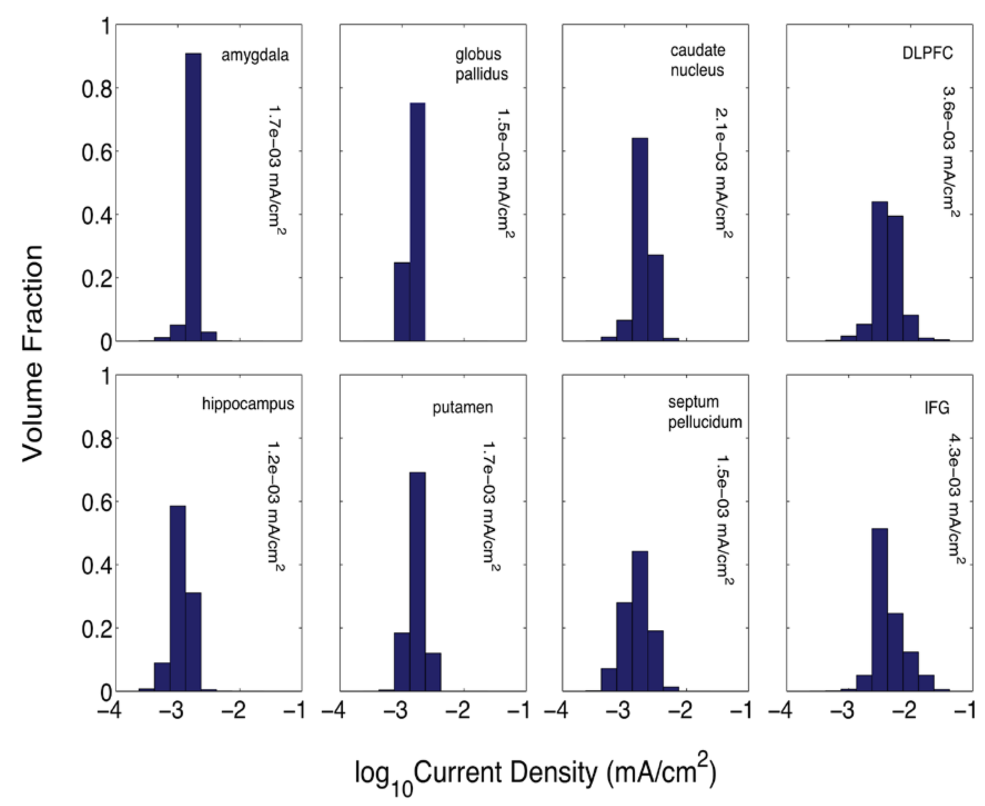

Figure 3. Current density distributions in brain structures for F3-RS montage at 1 mA using 22 cm^2 electrodes and composite white matter conductivity. Numeric values within each pane show the median current density within the named region.

The F3-RS electrode pattern produced large current densities in both left and right frontal and prefrontal regions, that is, it produced large currents under both stimulation and reference electrodes. To check this result, we simulated the effect of applying current between complementary (22 cm^2) electrodes placed at F4 and LS, using the composite white matter conductivity value.

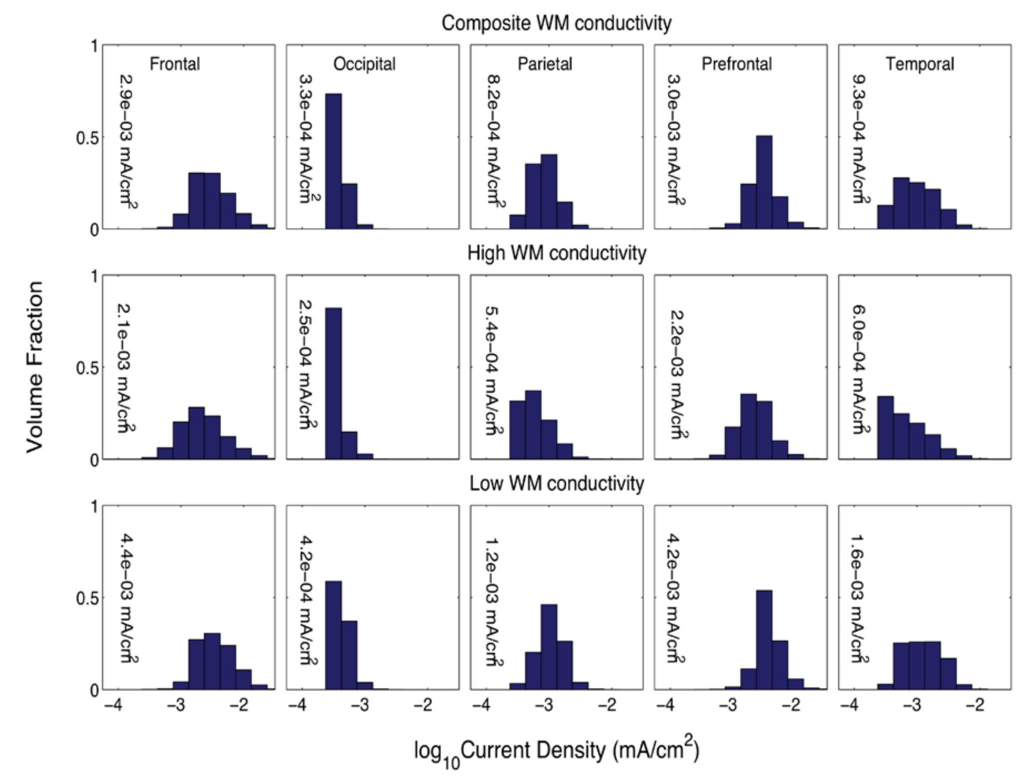

Figure 4. Current densities formed in brain regions as a result of assigning (top) composite white matter conductivity, (center) high white matter conductivity and (below) low white matter conductivity. Current applied at 1 mA using F3-RS montage, 22 cm^2 electrode area. Numeric values within each pane show the median current density within the named region.

Again, we found that all frontal and prefrontal current densities were large. In addition, overall median current densities in left frontal, and bilateral prefrontal regions were actually significantly larger for the F4-LS montage than for the F3-RS montage. Whereas median current densities in left DLPFC and IFG targets were similar and both significantly higher for F3-RS than F4-LS, current was differentially concentrated in the left DLPFC using the F4-LS montage .

Discussion and Conclusions

Both the F3-RS and F4-LS montages produced large current densities near both stimulation and reference electrodes, as expected. While the F3-RS montage produced large current densities in both the left IFG and left DLPFC, those formed by the F4-LS montage were larger in the left DLPFC, and overall current densities in both structures were higher using the F4-LS configuration. The distributions formed by F3-RS and F4-LS montages were not symmetric as expected, which most likely reflects the results of variability of conductivity distribution as well as electrode size and shape. It remains to be determined whether such variations in distributions truly occur in experimental situations, and whether the functional-neuroanatomic conclusions of such studies need to be altered. The F3-RS simulation together with the increased current density in left target areas found using the F4-LS montage does suggest that attempts to target the left inferior frontal gyrus might potentially also be achieved by the application of current to F4 and to the *left* supraorbital region, rather than to F3 and the *right* supraorbital region, as has been supposed. In addition, use of a F4-LS montage might be better employed to target the DLPFC. Current densities in DLPFC and IFG were as a result of the F3-RS montage were higher, although of the same order of magnitude as, those in other brain structures considered.

Literature Cited

Fregni F, Boggio PS, Nitsche MA, Bermpohl F, Antal A, Feredoes E, et al., 2005. Anodal transcranial direct current stimulation of prefrontal cortex enhances working memory. Exp Brain Res. 166, 23-30.

Iyer MB, Mattu U, Grafman J, Lomarev M, Sato S, Wasserman EM., 2005. Safety and cognitive effect of frontal DC brain polarization in healthy individuals. Neurology. 64, 872-875.

Nitsche MA, Paulus W., 2000. Excitability changes induced in the human motor cortex by weak transcranial direct current stimulation. J Physiol (Lond). 527(3), 633-639.

Sparing R, Mottaghy FM., 2008. Noninvasive brain stimulation with transcranial magnetic or direct current stimulation (TMS/tDCS) - From insights into human memory to therapy of its dysfunction. Methods., 44, 329-337.

Wagner T, Fregni F, Fecteau S, Grodzinsky A, Zahn M, Pascual-Leone A., 2007. Transcranial direct current stimulation: A computer-based human model study. NeuroImage. 35, 1113-1124.

Wassermann EM, Grafman J., 2005. Recharging cognition with DC brain polarization. Trends in Cognitive Science. 9(11), 503-505.

Zubal IG, Harrell CR, Smith EO, Rattner Z, Gindi G, Hoffer PB., 1994. Computerized 3-Dimensional segmented human anatomy. Med Phys. 21(2), 299-302.

For further information…

Please contact sadleir@ufl.edu. More information on this and related projects can be obtained at bioimpedance.bme. ufl.edu, where you can download a smaller-sized version of this poster.